EFFECT OF TALL BUILDINGS ON TURBULENT AIR FLOWS AND POLLUTION DISPERSION WITHIN A NEIGHBOURHOOD

Elsa Aristodemou[1,2], Luz Maria Boganegra[1], Dimitrios Pavlidis[2], Laetitia Mottet[2], Achilleas Constantinou[1], Christopher Pain[2], Alan Robins[3], and Helen ApSimon[4]

[1] School of Engineering, London South Bank University, London, UK.
[2] Department of Earth Sciences, Imperial College London, London, UK.
[3] Department of Mechanical Engineering Sciences, University of Surrey, Surrey, UK
[4] Department of Environmental Policy, Imperial College London, UK

Corresponding author: Elsa Aristodemou at: aristode@lsbu.ac.uk; e.aristodemou@imperial.ac.uk

Abstract:

A validated street-canyon/neighbourhood model is implemented to assess the effect of tall buildings on the dispersion of air pollution within a small complex of buildings. The work was motivated by both the increasing number of tall buildings in central London ("skyscrapers"), as well as the recent plans of placing Combined Heat and Power Plants (CHPs) within the urban environment; the work highlights the significance of modelling studies prior to any possible new building developments and the effect of building designs on the concentrations of pollutants. A new, open-source simulator, FLUIDITY, incorporating the Large Eddy Simulation (LES) approach, is implemented and the simulated results are validated against wind tunnel experiments carried out at the Enflo wind tunnel (University of Surrey). The wind tunnel experiments, with a seven-building configuration, were carried out to assess the effect of emissions from CHPs at the top of one of the buildings. The novel LES methodology implemented uses an unstructured, adaptive mesh and an anisotropic eddy viscosity tensor for the sub-grid scales (based on the anisotropic mesh). The comparisons of the normalised mean concentrations between model results and wind tunnel measurements show a good correlation – with errors ranging from 3 % to 30%, although at certain locations the error was higher. Following the validation procedure, two further hypothetical scenarios were carried out, in which the heights of buildings surrounding the source building were increased. The results showed clearly the effect of taller buildings on the surrounding air flows and dispersion patterns, and the generation of "dead-zones" and high-concentration hotspots in areas which did not previously exist. The work clearly showed that complex CFD modelling can provide useful information to urban planners when changed to cityscapes are considered, so that the optimal height of buildings - for minimal pollution effects - can be determined.

Key words: *air pollution, computational modelling, Large Eddy Simulations, urban environment, wind tunnel experiments.*

Summary of findings: Tall buildings have an immense impact on both the turbulent air velocity field and the dispersion of pollution within a local neighbourhood, with concentration hotspots generated in areas that previously were pollution free.

1. INTRODUCTION

Efficient, fast, and accurate urban dispersion predictions are necessary to assist with improving air quality within the urban environment through optimisation of critical infrastructure and control of emissions. Correct abatement policies require the understanding of the interaction of pollution from different emission sources at different scales, in a turbulent environment. Appropriate air pollution models involve the solution of non-linear equations (advective transport, chemical reactions, and turbulent diffusion) and require accurate predictions of spatial concentration gradients, as these influence the values of both the reaction rates as well as the transport of the pollutants. Achieving accurate predictions requires fine/high-resolution spatial grids - this has been a major issue over the last four decades, with adaptive grid methodologies appearing in the early 1990s by Benson and McRae (1991) resulting in the development of their Dynamic Solution Adaptive Grid Algorithm (DSAGA) on structured grids. Odman et al. (1997) followed with the implementation of an embedded Cartesian grid approach, whilst Tomlin et al. (1997) were amongst the first to implement an adaptive grid approach on an unstructured grid for two – dimensional problems. The adaptive algorithm of Benson and McRae (1991), DSAGA, was implemented by several authors in urban pollution problems since then, with Srivastava et al. (2000) using it in air quality models, capturing the changes in concentration distributions and their gradients due to advection as well as chemical reactions and dispersion of a pollutant puff (Srivastava et al. (2001a&b)).

In addition to the necessary high-resolution grids, determining the correct turbulent characteristics of the flow field and understanding the mixing processes and scalar exchange within and above canyons is also crucial in obtaining accurate predictions of the concentration levels (Zhoun and Hanna, 2007; Solazzo and Britter 2007). Turbulent flows in air pollution problems have traditionally been dealt with the Reynolds-Averaged Navier-Stokes methodology (RANS), and the well-established k-epsilon turbulence model. However, studies by Coirier et al. (2005) and Sabatino et al. (2008) showed that the turbulent kinetic energy was under-predicted and it was suggested that determining the correct turbulent parameters in the k‒epsilon turbulent model is more important than grid refinement for obtaining accurate turbulent flow predictions.

One of the principle concerns in street canyon pollution studies is the transfer of pollutants from within the canyons to the external shear layer at the top of the canyon. In the past, for the two-dimensional canyons, this transfer has been assumed to be directly proportional to the external velocity (Operational models such as the Operational Street Pollution Model (OSPM)). However, numerical studies by Baik and Kim (2002) showed that both the vertical turbulent velocities and the vertical mean velocities are important. They found that pollutants escape from the street canyon mainly by turbulent processes and that the net effect of mean flow is to make some escaped pollutants to re-enter the street canyon. They also showed that different inflow turbulence intensities, inflow wind speeds and aspect ratios confirm these findings. A similar study was carried out by Caton et al. (2003) where the authors investigated both analytically and experimentally the dispersion mechanisms in such a two-dimensional canyon. The essential outcome of their study was to show how the transfer of pollutants at the top of the street canyon depends not only on the external mean velocity but also on the turbulent properties of the incoming flow, and should thus be included in any operational model. The effect of the turbulent intensity conditions at the inlet on the dispersion of the pollution within the street canyons is also discussed in Kim and Baik (2003). In this study the authors describe how the pollutants are transported upwards or downwards, depending on the strength of the eddy diffusion and advection at different heights, and the influence of the main and secondary vortices. The authors confirmed that as the inflow turbulent intensity increases, the pollutant concentration in the street canyon becomes low and the upward escape of pollutants from the canyon is facilitated. The importance of the inlet turbulent conditions for the accurate prediction of mean concentrations is also highlighted in the study of Milliez and Carisimo (2007). The authors also highlight the importance of the turbulence model parameterisation chosen for their k-epsilon model (RANS) in the simulated mean concentrations and fluctuations and their variance. Their sensitivity studies on the fluctuations in the source emission rate showed little effect. The RANS studies by Coirier et al. (2005) and Sabatino et al. (2008) showed that the turbulent kinetic energy was under-predicted and it was suggested that determining the correct turbulent parameters in the k‒epsilon turbulent model is crucial, and perhaps more important that the grid-refinement. The authors also make the interesting comment that should the need for short-term responses arise for risk assessment purposes, it would mean that peak concentrations must be evaluated, which can be only achieved more appropriately using methodologies such as the large eddy simulations (LES).

The LES method is currently one of the most favoured and powerful approaches for simulating complex turbulent flows as it enables the capturing of the unsteadiness of the flow (and thus providing detailed information of the flow structures as well as of the turbulence statistics) leading to a greater understanding of the physical processes taking places within street canyons. The strength of LES lies in the fact that, in contrast to both the DNS and the RANS approach, it is able to simulate the large-scale turbulent structures explicitly whilst the smaller-scale structures are modelled. It was first proposed by Smagorinsky (1963) for atmospheric flows and since then it has been facilitated by the rapid growth in computing power, thus enabling it to enter mainstream engineering. Zhiyin (2015) presents a detailed review of the method, outlining its progress since its initial appearance in the 1960s and how it has entered mainstream engineering in the last two decades. In addition, the author describes the challenges, past and present for the LES method, with regards to the range of turbulent length scales it has to represent during transient simulations, as well as the theoretical developments that have been carried out over the years in order to represent turbulent inlet conditions, and subgrid scale models. Modelling the smaller structures requires some assumptions and parameterisations and the subgrid scale model has been traditionally based on the well-known Smagorisnky-type eddy viscosity model (Smagorinsky, 1963). In the initial version of the model, the Smagorisnky coefficient required for the determination of the eddy viscosity was kept constant. However, it was soon recognised that this assumption leads to over-dissipation of the sub-grid scale turbulent kinetic energy, and thus efforts since the 1990s have taken place resulting to the development of a large number of sub-grid scale models, based on three main categories: (a) eddy-viscosity methods, (b) similarity models, where the sub-grid scale model is deduced from the stress tensor of the resolved field by applying filtering methods, and (c) mixed models, which have an eddy-viscosity component added to the similarity expressions.

In addition to the variety of sub-grid scales models within the LES approach, adaptive grids were also implemented, with one of the earliest implementations being the work of Wissink et al. (2000) with a Cartesian Adaptive Mesh Refinement (AMR) capability. This was followed by the work of Ghorai et al. (2000) where we also see an implementation of a three-dimensional, time-dependent gridding technique for dispersion problems in neutral, stable, and unstable atmospheric boundary layers. Walton and Cheng (2002) implemented LES using a structured grid, for street canyons in Hong-Kong, with an aspect ratio (Height/width) of 1.2. A dynamic LES subgrid-scale model was implemented, together with period boundary conditions. Based on the comparisons between simulations and wind-tunnel data, the authors concluded that, in contrast to Baik and Kim's (2002) work, it is large scale turbulent eddies that remove pollutants from the canyon rather than a steady diffusion resulting from small scale turbulence. The authors also found that LES predicts a noticeably higher turbulence kinetic energy in the vortex core, leading to improved mixing and dispersion compared to RANS results. An interesting and informative study of *reactive* pollutants (NO and NO_2 and O_3) using the LES approach is described by Baker et al. (2004) which looks at the spatial variation of these contaminants in an idealised street canyon configuration. Their results showed that concentrations of NO and NO_2 were higher in the leeward direction than in the windward, being consistent with the simulations results of Baik and Kim (2002) and the field measurements of Xie et al. 2003. The primary vortex is believed to be responsible for the entrainment and dispersion of traffic emissions. The authors also found that a strong shear layer also leads to the "trapping" of the pollutants. At the locations where the shear layer destabilises, thus becoming more turbulent, a greater air exchange occurs between the canyon and the air above, thus resulting in lower concentration gradients, and a "smoother" concentration distribution. The work of Porte-Agel (2004) discusses the development of the varying versions of the dynamic Smagorinky LES models, and comparisons with experimental data within the atmospheric boundary layer. Fully three-dimensional dynamic grid adaptivity for air quality models is relatively new. Constantinescu et al. (2008) show that high resolution grids are needed both near the emission sources of pollution as well further upwind, whilst Aristodemou et al. (2009) implemented and validated an adaptive LES method using mean flows and fluctuations against wind tunnel data.

More recent studies discuss CFD applications for urban micro-climate, incorporating heat island effects as well as the effect of building layouts and presence of upstream buildings to the downstream ones. Toparlar et al. 2015 implements unsteady RANS simulations to study the heat island effects through heat transfer by conduction, convection and radiation in a case study area in Rotterdam (Netherlands), whilst Cui et al. (2016) discuss the effect of the presence of an upstream building to indoor pollution levels in a downstream multi-story building. Gromke et al (2015) study the effect of green-infrastructure (avenue-trees) on the natural ventilation and air quality through a series of RANS-based CFD simulations which included the aerodynamics effects of not only the buildings, but also of the avenue trees. A complex modelling study looking at the effects of building layouts and tree arrangements on the thermal comfort at pedestrian level has been carried out by Hong and Lin (2015); their modelling simulations considered an air flow model, vegetation model that incorporated the amount of heat absorbed by leaves, as well as the amount of heat convection taking place, and the process of transpiration by the leaves. Their study emphasises the importance of using numerical studies /modelling for optimising building design layouts together with the green infrastructure for the optimal thermal comfort within the urban environment, as well as the reduction of pollution levels. The effect of outdoor air pollution on indoor air quality, for either naturally or mechanically ventilated buildings has also been gaining momentum the past few years, highlighting the importance of improving outdoor air quality. One such study has been carried out recently by Tong et al. (2016), which implemented CFD simulation in order to assess the effect of various building parameters/design and ventilation strategies for improving indoor air quality, particularly with respect to aerosols/particulate matter. The effect of green infrastructure/urban vegetation on the deposition and dispersion of pollutants in the urban environment is also of great interest to both researchers as well as urban planners. A very useful recent review of the topic has been carried out by Janhall (2016), identifying which types of vegetation would be most appropriate and at what locations they should be placed within the urban environment for enhancing the deposition and dispersion of specifically particulate matter.

The many applications and attempts for modelling dispersion of pollutants within our urban environment thus far emphasise the importance of the continuous endeavours to improve the accuracy of the predictions. Immense progress has been achieved so far, and the preceding studies show that it is widely recognised that in order to improve the accuracy of the predictions, and in order to capture the turbulent effects of the flow on the dispersion of the pollutants (at the short timescales that have an effect on human health) an adaptive grid is needed, although less-computationally intensive models have also been developed and implemented recently in order to address the emergency-response scenarios (Zhang et al.

2016). In this work, the exploration of adaptive LES on unstructured grids for urban pollution problems is continued, with the main aim of studying in detail the effect of changing the building heights on the dispersion of the pollutants within cities.

2. METHODOLOGY

Modelling realistic urban flows requires a compromise between the steady-state RANS method and the computationally-intensive direct numerical simulation (DNS) method (Coceal et al. 2007). This is achieved through the gaining popularity large eddy simulation (LES), especially when adaptive-meshes are employed (Pope, 2000). The methodology implemented was initially developed by Bentham (2004), and combines a Smagorinsky-type sub-grid-scale turbulence model, with a fully adaptive unstructured mesh that optimizes the numerical resolution (finite element sizes) throughout the flow. Transport of pollutant concentrations is determined by a high-resolution method which is globally high order accurate in space and time and is designed for use with unstructured finite element meshes (Pain et al., 2001). The advection scheme provides robustness and may even be used as an alternative to traditional LES models (e.g. providing additional dissipation) for the pollutant concentration or momentum fields. The model employs a world-leading anisotropic mesh adaptivity method based on mathematical optimization as described in Pain et al. (2001). This method adapts tetrahedral elements to resolve all flow variables, e.g. velocity, pressure, particle concentration, by producing long-thin (anisotropic) elements with large aspect ratios where the physics dictates, such as in boundary layers. This can achieve great computational efficiency for large transient 3-D fluid flow problems and is fully exploited in the computationally demanding urban flows modelled here. For large problems, a tetrahedral-based parallel adaptive-mesh method described in Gorman et al. (2003) is exploited to achieve highly detailed turbulence model results. With the non-uniform adaptive resolution and use of parallel computing, varying building scales can be resolved. Our methodology has been validated against wind tunnel data (Bentham, 2004; Aristodemou et al. 2009; Boganegra, 2016) as collected in the Enflo wind tunnel (Robins, personal communication, 2013). The Enflo wind tunnel has been used successfully in many studies of atmospheric air flows and dispersion (Carpentieri and Robins, 2015; Belcher et al. 2015) and measurements from one of these experiments is being utilised in the current study.

2.1 The Mesh-Adaptive Large Eddy Simulations and Boundary Conditions

The LES equations implemented in this work are based on the theoretical work developed by Bentham (2004) and Pain et al. (2001) as found within the FLUIDITY software (http://fluidityproject.github.io/), in which a key aspect was the anisotropic eddy viscosity subsgrid scale model. The basic equations are given in Appendix A and further details can be obtained from Bentham (2004) and Pavlidis (2010). The computational domain was based on the wind tunnel configuration representing the seven buildings as shown in Fig. 1, with initial building dimensions as used in the wind tunnel (Fig. 2a, Table 1). Additional scenarios were run with (i) increasing the building heights of all buildings except building A (Case 2, Table 1, Fig. 2b) and (ii) All building heights as in Case 2, except for building F, which is increased (Case 3, Table 1, Fig 2c). The tracer source was placed at the top of building A, at coordinates (-0.01875 m, 0.01875, 0.1508m). The dimensions of the computational domain were based on the building dimensions within the wind tunnel, and covered a volume of 4.0 m by 2.0 m by 2.0 m, allowing a long-development section for the formation of a deep boundary layer. The simulations were carried out with both: (i) a constant velocity inlet condition, and (ii) a turbulent velocity inlet of a constant velocity inlet condition (left boundary of the domain) so that an assessment of the effect of the inlet conditions could be made. The downstream boundary (outlet) was left as pressure boundary (no-stress condition), whilst the remaining boundary conditions consisted of: (i) no-slip condition for the solid walls of buildings and "floor" of domain, and (ii) no-shear conditions for the free surfaces (sides and top).

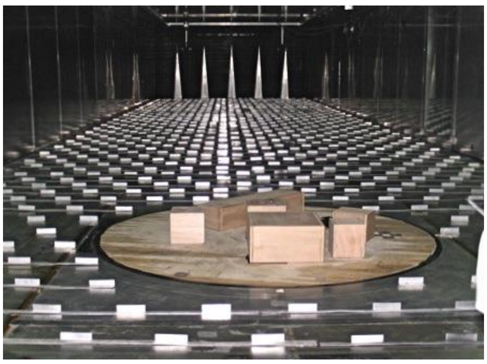

Figure 1 The building configuration in the Enflo wind tunnel, University of Surrey, UK (Robins, 2013)

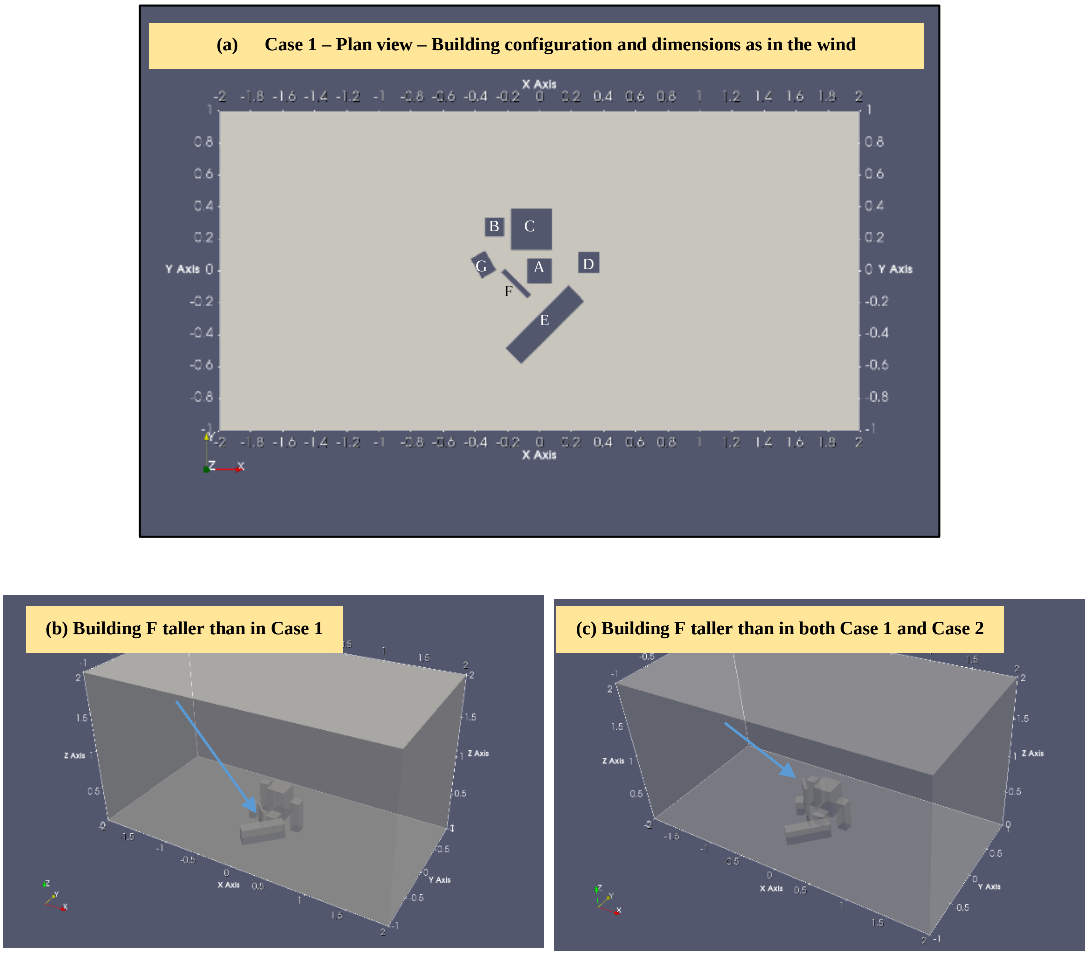

Figure 2 The building configuration in the computational FLUIDITY simulations: (a) Plan View of all buildings for Case1 configurations – with dimensions as in the wind tunnel; (b) Case 2 configuration – all buildings with higher heights except building A; (c) Case 3 configuration – heights as in Case 2 except for the much taller building F. *Note: All heights given in Table 1; dimensions in metres.*

2.2 Mesh adaptivity

One of the key and innovative aspects of the FLUIDITY software is its mesh-adaptivity capability; the mesh-adaptivity capability on unstructured meshes within FLUIDITY makes it a unique tool which enhances and provides detailed and accurate information at high resolutions within the computational domain. The process of adaptive re-meshing consists of three parts: (i) deciding what mesh is desired; (ii) generating this mesh; and (iii) transferring data from the old mesh to the new mesh. The form of communication between the first two stages is a metric: a symmetric positive-definite tensor field which encodes the desired geometric properties of the mesh (Fluidity manual, 2016). The process allows changes to be made to the mesh according to a functional whose value can lead to: (i) edge collapsing (hence reduces number of elements and nodes – hence mesh coarsening); or edge splitting (hence mesh refinement); or node movement (hence mesh smoothing without altering the number of nodes or elements). The adaptivity options within FLUIDITY are based on *a posteriori error* estimates, which when computed are used to modify the discretisation to achieve some error target. These include *h-adaptivity*, which changes the connectivity of the mesh; *p-adaptivity*, which increases the polynomial order of the approximation; and *r-adaptivity*, which relocates the vertices of the mesh while retaining the same connectivity (Fluidity Manual, 2016). A combination of these can also be set e.g. *hr-adaptivity*, which was implemented in this study. Adaptivity options can be field-specific (i.e. different fields computed fields can be configured with their own specific adaptivity options) but also non-field specific options can be set.

For the simulations in this study, field-specific adaptivity options (Interpolation Error bound value, as well as the type of interpolation) were assigned to the velocity (vector) field and the tracer (scalar) field. For the velocity field (vector), the interpolation error bound value was set to the vector value of [0.05, 0.05, 0.05], whilst for the tracer, the scalar value of 0.01 was assigned. For both fields the type of interpolation was set to the "consistent interpolation" option. For the more general non-field adaptivity options, mesh resolution can also be controlled through the specification of the minimum and maximum element sizes in each direction, with different size limits set in different regions of the computational domain. In our simulations, these were set to the values of: element-minimum =0.003m and element-maximum=0.004m, around the location of the sources, on top of building A; hence, mesh-resolution can be "forced" in specific regions of the domain. In addition, the frequency of the adaptivity process can also be controlled by the user – with adaptivity taking place every so many timesteps, as opposed to at every time step. For this study, the mesh was adapted every 15 timesteps. Anisotropic gradation was also allowed in the simulations, with a tensor gamma filed having diagonal values of 0.75. An adaptive time-step was also used throughout the simulations, based on a CFL number of 0.9. The maximum number of nodes can also be set; for our simulations, this was set to 400,000 nodes, rendering approximately ~1,000,000 elements. Absolute and relative convergence errors were set to 10^{-12} and 10^{-7} respectively. Further details on the method of mesh-adaptivity and the metrics used can be found in Pain et al. (2001), as well as the FLUIDITY manual (2016), with applications for air pollution problems in Bentham (2004), Aristodemou et al. (2009), Pavlidis (2010), and Boganegra (2016). An example of the adaptivity effect on the computational mesh can be seen in the examples in section 3 (Results section).

2.3 Wind tunnel Experiments

The wind tunnel experiments, representing different building configurations, were carried out at the Enflo wind tunnel (http://www.surrey.ac.uk/mes/research/aef/enflo/) (University of Surrey), and the complete data set were provided (Robins, 2016, personal commun.). A total of eight cases were tested representing different building configurations, with the number of buildings varying from 1 to 7. The work presented here represents the "all-buildings" configuration in which all seven buildings were considered. Reference wind velocity was taken to be 2.1 m/s, and mean concentrations of the passive tracer were measured using the state-of the art sensors. The model atmospheric boundary layer, for neutral atmospheric conditions, was generated using vorticity-generating spires at the upstream/inlet part of the tunnel, whilst roughness elements were placed on the floor (h_{rough}=0.025m). Tracer emission was set-up on top of one of the buildings (Fig. 2a - Garden building – A) and measurements were taken for four different wind directions – although comparisons in this study were carried out for only one wind direction.

2.4 Velocity Inlet Boundary Conditions

Measurements of the developed velocity profile were taken downstream of the spires-inlet, with the measured normalised mean velocity values as shown in Fig. 3 (a). Similarly, the Reynolds stresses in all directions were also measured (Fig. 3b) and both sets of data (mean velocity profile and Reynolds stresses) were utilised as inlet boundary conditions in the LES simulations. The turbulent inlet velocity boundary was subsequently being generated based on the synthetic eddy method of Jarrin et al. (2006) and as implemented in the FLUIDITY LES model by Pavlidis (2010).

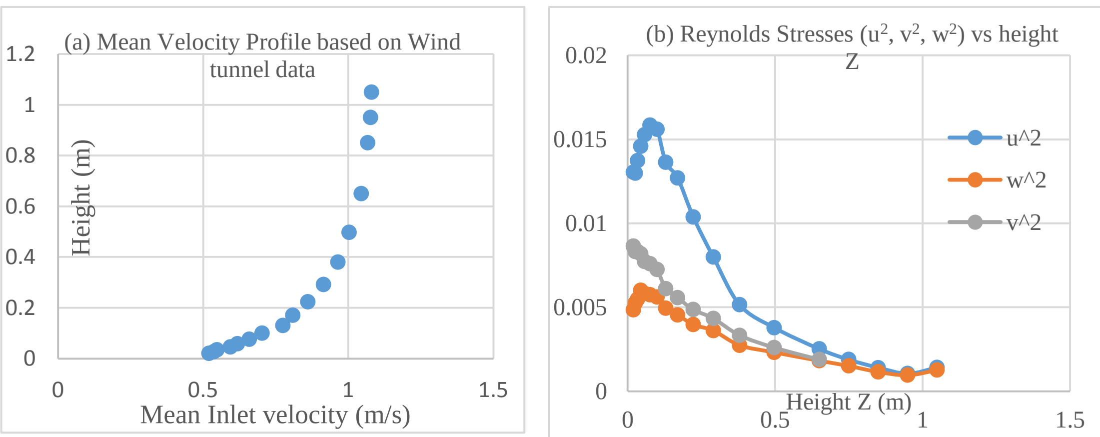

Figure 3 (a) The velocity profile as measured in the wind tunnel and as represented in the computational simulations; (b) the Reynolds stresses (in the x, y and z directions) as measured in the wind tunnel and as represented in the computational simulations.

3. RESULTS

3.1 Comparison of LES results with wind tunnel data.

The LES simulations were carried out on the Dell Precision Tower 7810 computer, with a dual Intel Xeon Processor for a total simulation time of ten seconds, corresponding to the same amount of real time i.e. real time of ten seconds. The main simulated variables over time are: (i) pressure; (ii) velocity (each component); tracer concentrations for each tracer source. The normalised mean concentrations from the LES simulations – at several detectors - were subsequently determined, and compared with the measured wind tunnel data (normalised mean concentrations).

The LES simulations were run with *three* different velocity inlet conditions: (i) a *constant velocity inlet*, with a velocity of 1.0 m/s, and no specification of turbulent characteristics; this was the simplest inlet boundary condition to be considered, and it was implemented for comparison purposes; (ii) a *Turbulent-Inlet-1* condition, representing a logarithmic inlet velocity profile very similar to the measured wind tunnel profile, and a hypothetical set of Reynolds stresses lower than the wind tunnel ones; (iii) a *Turbulent-Inlet-2* condition, representing again a logarithmic inlet velocity profile as measured in the wind tunnel and with Reynolds stresses as measured in the wind tunnel (Fig. 3). The comparisons are shown in Fig. 4 for several detectors within the domain. The detectors were placed along different x-lines (different x-coordinates), to the right of buildings A and C, and between buildings A, C, E and D, with some detectors beyond building D (detectors 197 to 205, with x=0.433 and detectors 251 to 286 with x=0.751m); the detectors were grouped together according to their height, and their x-co-ordinate, with only the y-coordinate varying in each set; the height of detectors ranged from z=0.065m (almost half the height of the building A) to z=0.3 m (just over twice the height of building A; recall: the source height is at 0.1508 m). The set of detectors to the right of building C (with x=0.203m) at low heights (Z=0.065 m) showed greater inconsistency between simulations and measurements and this could be due to the less accurate determination of the turbulent field in those locations. A summary of the percentage errors between measurements and simulations –with errors ranging between 3% to 30% - is shown in Table 1b.

From the results, some very interesting observations can be made: (a) the inlet conditions played a major role in the comparisons for the detectors within the building-area, with the *constant velocity inlet* scenarios resulting in the worst correlations between wind tunnel data and simulated results for these detectors (D89 to D106, D152 to D160, and D197 to D205); however, when the inlet was represented with the turbulent characteristics as measured in the wind tunnel the correlations were improved considerably for these detectors, capturing both the overall trend variation along specific lines of detectors, as well as the magnitude of the concentrations. The best correlations between measurements and simulations (for detectors within the building area) were based on the *Turbulent-Inlet-2* simulations, indicating that the LES simulations capture the complex turbulent flow field, and hence the mean tracer concentrations; (b) very interestingly, for certain detectors well away from the building area (x=0.751 m) and for heights (z=0.3) well above the source (detectors D278 to D286) the *constant inlet* simulations gave the best comparisons with the wind tunnel data; (c) for detectors again away from the building area but at lower heights (detectors D251 to D259 and D260 to D268) the simulation results from the three different inlet conditions were very similar – showing that at some locations away from the building area, the inlet conditions have no significant effect on the final result - the mean simulated concentrations were very similar for the three different inlet conditions.

3.2 Effect of tall buildings on the local turbulent air flows and dispersion/concentration of air pollutants.

The main interest of the study was to investigate the effect of tall buildings on the local dispersion of pollutants in an area of interest, particularly when the source of pollution resides at the top of a “normal-height” building (wind tunnel height of 0.1428 m, corresponding to real building height of 28.56 m using a scale factor of 200) that is surrounded by taller buildings. Two additional hypothetical scenarios (Case 2 and Case 3) were considered in which the heights of all buildings (as shown in Table 1) were increased (relative to the wind tunnel case), except for the building where the source was located on (Building A -

Garden building). The turbulent air flow patterns and dispersion of pollutants for all three cases are shown in Figs 5 to 8. Results are shown for three plane orientations: (i) Horizontal plan view at source height; (ii) The X-Z vertical plane through the centre of the domain and (iii) the Y-Z plane through the centre of the domain. It is noted that the source is located at the top of building A (Garden building) at height z=0.1508 m.

Fig 5a: Horizontal Plan view at Z=0.1508m - Velocity fields for the three cases.

The velocity results are shown in the wireframe representation - so that the mesh can also be seen. It is clear from the results that the hypothetical scenarios with taller buildings (Case 2 and Case 3) have different dominant flows and re-circulation patterns when compared to the wind-tunnel case (Case 1), influencing the subsequent direction of dispersion. For Cases 2 and 3, there are low-velocity regions around buildings A, C and D, and also downstream of building E. For Case 2, there is slightly higher velocity surrounding building D than in Case 3, which results to lower concentrations – as will be seen in Fig. 5b.

Fig 5b: Horizontal plan view at Z=0.1508m - The dispersion patterns and concentration fields for all three Cases – with the corresponding adaptive meshes.

Fig 5b shows the dispersion results for all three cases together with the very detailed adaptive mesh, required for capturing accurately both the turbulent flow patterns as well as the dispersion patterns at high spatial resolution.

<u>*Case 1:*</u> The dominant dispersion pattern for Case 1 is towards the right of building A and this reflects the predominant main flow direction, with very little circulation at that height. However, as soon as the heights of the buildings surrounding the source building (building A) are increased, the flow patterns change, with different circulation patterns developing and thus directing the pollutant (in varying degrees) around buildings C and D, E and F, as seen in Cases 2 and 3.

<u>*Case 2:*</u> the pollutant is “pushed” towards building C and at the front of building D, as well as in between the two buildings, reflecting the weaker velocity field in this region; the pollution also accumulates towards building F, as the velocity recirculation is weak in this region too, with thus, concentrations are strongest in these locations. Concentrations are lower also between buildings D and E.

<u>*Case 3:*</u> however, when the height of building F (Garage building) is increased further, the circulation flow patterns are affected dramatically; the presence of the taller F-building, generates a stronger circulation pattern between buildings A, C and D, and thus pollution concentrations in front of building C are now virtually non-existent, and pollution seems to concentrate more on top of the building A, and around building D. The lower concentrations between Buildings A and C reflect the stronger velocity field generated between these buildings, due to the presence of the taller F-building. Similarly, a stronger flow field exists between buildings F and E, with virtually no pollution in the region between these buildings (F and E). However, a build-up of pollutants occurs around the top building A, which finds an “escape” route through the gap between buildings D and E, and also between buildings C and D; most of the pollution seems to concentrate around building D.

Thus, comparing the three cases in a horizontal plane, at the height of the source, it is clear that when the heights of the buildings around the source building are increased, higher concentrations are accumulated between the surrounding buildings (C, D, E, and F), with buildings C and D being particularly affected. Case 2 seems to be the worse configuration/design (in terms of building heights), as more buildings are affected by higher surrounding concentrations. In Case 3, only building D is substantially affected together with the region between building A (the source-building) and D.

Fig 6a: Vertical Plan view (X-Z) through centre of domain (Y=0.0m) - The Velocity fields for all three Cases.

Fig 6a shows the velocity fields generated in the three cases – in magnitude representation. Looking at the turbulent flow fields in the X-Z vertical plane, it is clear a distinct difference exists between the cases, with interesting velocity patterns and “dead-zones” being generated because of the presence of the taller buildings – especially for Case 3, in which the F-building is very much taller than the other two cases (0.6 m as opposed to 0.0315 m in the wind tunnel case). This increased height generates an interesting “dead-zone” immediately downstream of building F, but also an interesting circulation pattern in the central area and above building A (source building), with a strong velocity path moving towards the right of the domain above building A, and towards building D. This has a major effect on the dispersion as it will be seen in Fig 6b.

Fig 6b: Vertical Plan view (X-Z) through centre of domain (Y=0.0m) – The Dispersion patterns and concentration fields for all three Cases.

The effect of the velocity fields generated by the taller buildings as shown in Fig 6a – for Cases 2 and 3 – are clearly seen in the dispersion and concentration values of the pollution.

Case 1: It is clear the pollutant is concentrating mostly on top of building A; also to the right side of building A, and above building D. The flow field is very weak between buildings A and D, and hence concentrations are higher between these buildings filling up most of the area between the two buildings. The pollution plume also forms above building D and stays persistently at that height (~0.12m) for quite some distance away from the building (from x=0.4 m to x=0.8m), beyond which concentrations begin to increase at lower heights; up to that horizontal distance of x=~ 0.8m and for heights lower than 0.12 m, the region beyond building D is pollution free. For distances beyond x=~ 0.8 m, pollution seems to concentrate substantially at lower levels to the end of the computational domain. This is quite different for Case 2 and Case 3.

It is interesting to notice that although the pollution concentrates above and around the building A, none of the pollution finds its way to the left of building A i.e. in regions between buildings A and F or A and G, despite the weak flow fields in these regions; obviously this is due to the main flow direction, with air moving from the left to the right of the domain, and as buildings F and G are lower (building F) or comparable in height (building G) to building A, the main flow direction is not affected, hence allowing these regions to be pollution free.

These pollution-free regions, however, are not sustained, when the heights of the buildings surrounding building A are increased, as can be seen in Cases 2 and 3.

Case 2: It is clear from the results that the increased heights of buildings G, F and D surrounding building A have an adverse effect on the pollution concentrations around mainly buildings A and D. The regions between buildings G, F, and A are still unaffected (as in Case 1); however, the regions between buildings A and D are affected negatively; in the first instance, higher concentrations are now observed over the whole of the top of building A (as opposed to only the right side of it – Case 1), and although the region between buildings F and A is not affected, the higher concentration towards the left of the building A is not considered a positive thing. Higher concentrations are also now observed just on the right-hand side of building D; these high concentrations did not exist before (Case 1), as building D was much lower, and the pollution plume was moving above the building height. However, increasing the height of building D has led to an accumulation of pollution around its right wall. These results have implications for the urban/city design point of view, as they imply that residents in building D will be affected by higher concentrations at this particular height, as opposed to residents at higher levels.

Similarly, a second striking difference between Case 2 and Case 1 is also the accumulation of pollution in the region just beyond building D. We recall that in Case 1, this region close to building D and up to the horizontal distance x=0.8 m - was pollution free. This is no longer the case; the increased heights of the buildings surrounding building A have a detrimental effect on pollution concentrations in regions close to the buildings which again have implications for the urban/city design.

Case 3. Increasing the height of building F even further, whilst keeping all the remaining heights the same as in Case 2, created some very interesting flows (as seen in Figs 14 and 15) and dispersion features, as seen in Fig. 16. The most striking differences between all cases is the stronger accumulation of pollution just on the right of building D. These concentrations were lower in Case 2 and non-existent in Case 1. Pollution also seems to now accumulate on the right side of building F – a region that was completely pollution-free in both Case 1 and Case 2. This is due to the low-velocity field generated around building F – due to its height – as already clearly seen in Figs 14 and 15. This is a completely new feature observed in Case 3, which did not exist in either Case 1 or Case 2, indicating how the increased height of building F allows the accumulation/trapping of pollutants at certain heights. This again has immense implications on the urban/city design. It is important to note that the region between building F and A, for heights below the height of building A is unaffected by pollution – it is still pollution free, as in the previous

Cases 1 and 2; it is only at the higher levels that pollution accumulation is observed, reflecting the flow fields that are generated at the higher levels.

The comparisons of the results for the three cases in this vertical, X-Z plane was very interesting and informative; they clearly showed how greatly the increased heights of the buildings around the source building have affected the distribution of pollution, with Case 3 being the worst case, as higher accumulation of pollution occurred in regions, which were previously pollution-free.

Fig 7a: Vertical Y-Z plane through the centre of the domain (x=0.0 m) – Velocity fields

The velocity fields generated in the three cases – in magnitude are shown in here. The Y-Z plane is normal to the incoming velocity vector (x-component only) and viewing results in this plane allows us to see the results between buildings E, A and C only, due to the configuration of the buildings; unfortunately building F, whose height changes dramatically between Cases 1, 2 and 3, is not seen in this plane; however, its effect is observed in both the velocity fields and pollution patterns, particularly for Cases 2 and 3.

Case 1: The velocity field is relatively simple, with some recirculation occurring between buildings E and A, and between A and C, and the higher flows above the buildings – following the logarithmic velocity profile.

Case 2: Interesting flow patterns begin to develop between the buildings, as soon as the heights of buildings E and C are increased. Higher velocities develop n the right of building E, whilst a recirculation zone seems to exist above the buildings A, and E. The "uniform" velocity profile that seems to be observed in Case 1, for heights above 0.15 m is now disturbed and stronger velocity dead-zones appear around buildings A and C, which have a direct effect on the dispersion of the pollution.

Case 3: Even stronger and more interesting velocity patterns are developed in this case, due to the increased height of building F (although not seen in the cross-section), especially above building A; a velocity "dead-zone" is formed to the left of building A, between heights 0.25 m to 0.6 m, consistent with the "dead-zone" observed in the X-Z plane (Fig 6a). In contrast to this "dead-zone", a strong velocity field is form diagonally between buildings A and C, directly affecting the pollution distribution – as seen in Fig. 7b.

Figs 7b and 7c: Vertical Y-Z plane through the centre of the domain (x=0.0 m) – Dispersion patterns with the Adaptive meshes.

The dispersion results, together with the associated adaptive meshes are shown here – highlighting the detailed capturing of the evolved dispersion patterns and the associated adaptive meshes.

Case 1: The results in this case are very simple, indicating the spread of pollution on top of the building A - at a relatively small height above the building; all other regions (between buildings E and A, and between A and C) are pollution free. The velocity fields show the high flows above the buildings, with little recirculation patterns amongst the buildings. In a way, not much seems to be happening, except on top of the building A.

Case 2: An interesting spread of pollution occurs vertically and above building A, as well as towards building C and at heights above the height of building. Pollution seems to be accumulating on the walls of building C – for heights above building A - as it could also be seen in the horizontal plane (Fig 5b). The increased height of buildings C and E had the effect of "blocking" the pollution on the left side of building C – and also increased the concentrations over the whole of the top of building A; increased concentration levels in the region between the buildings E and A, and at heights above the building A - which was a pollution-free region in Case 1 – can also now be seen. Some pollution levels are also detected on the right side of building C.

Case 3: The most interesting pollution feature in this case is the vertical spread of pollution for heights well above the height of building A – and in the region between building A and E. High concentrations are seen rising well above the height of the two buildings – in the region between them - and mostly to the left of building A, due to an interesting low velocity region "engulfed" by high velocity fields. This feature can be seen/discussed in association with the pollution spread in the horizontal plane (Fig 5b) where the spread of pollution around building A is seen. Results in Fig 7b show the extend of the vertical spread of pollution, due to the interesting low velocity field within this region.

A striking feature for this case is the high velocity trend developed between buildings A and C (almost diagonally from the centre of the top of building A towards building C) (Fig 7a(iii)) which eliminates a concentration hotspot on the left of building C - contrary to what was seen in Case 2. No concentration hotspots are observed at levels below the height of building A, in the region between buildings A - contrary again to what is seen in Case 2.

These results, especially for Cases 2 and 3 emphasise the importance of the height of buildings within the very localised regions around them; they show increased pollution levels in such regions which were previously pollution free – these pollution hotspots occur in different locations and different heights within the domain; this implies that detailed CFD studies can guide the urban designers/city planners for the optimal building heights so as to minimise people's exposure to high concentration levels.

Fig 8 Concentration Iso-surfaces for Case 1 and 3.

This figure shows clearly the difference in the overall dispersion and concentration pattern of the dispersion due to the varying building configurations. Fig 8a shows the pollution dispersing at a long distance away from the building area, whilst as soon as tall buildings surround the emission building A, the pollution remains within the building area and around buildings A and D – Fig 8b.

CONCLUSIONS

Complex turbulent air flows and pollution concentrations have been accurately captured using an LES approach with a novel anisotropic eddy viscosity model, and compared with wind tunnel data for a specific 7-building configuration; good correlations of the normalised, mean concentrations between experimental data and simulations were achieved and further simulations were carried out in order to assess the effect of increasing the building heights surrounding an emission source on the pollution concentration levels within the domain. The results clearly show how increasing the building heights of the buildings around an emission source has a detrimental effect on pollution levels within specific regions of the domain that were initially pollution-free. Two hypothetical cases were studied which showed clearly that pollution levels increased at higher levels and in regions between the new buildings, creating new concentration hotspots. This was a direct effect of the interesting velocity fields developed within the area of interest, which consisted of several low-velocity zones – due to the introduction of tall buildings.

These results highlighted the importance of detailed air flow and dispersion modelling within an urban environment prior to any new building developments that would involve high/tall buildings. The changing cityscapes due to the continuous rise of such tall buildings and the possibility of emission sources within the urban environment (due to the presence of CHPs) necessitates such detailed computational and physical modelling in order to optimise the design of the new buildings and minimise the exposure of the urban population to harmful air pollutants. As it is seen from the results, simply changing the height of a single building can have serious, negative effects on the pollution concentrations in regions were previously pollution-free. Thus, assessing the effect of building designs/heights through complex modelling and optimising both the locations as well as the dimensions/outlines is a necessity in order to sustain a healthy urban environment.

Acknowledgements

This work was initiated by a Master programme within the Environmental Policy Centre at Imperial College London, followed by further computational modelling work using the Imperial College FLUIDITY software within the School of Engineering at LSBU, as part of the Masters dissertation by Luz Boganegra. The wind tunnel measurements were carried out at the Enflo wind tunnel at the University of Surrey. This work currently forms part of the EPSRC MAGIC project No: P58094.

REFERENCES

Aristodemou, E., T. Bentham, C. Pain and A. Robins: 2009. Atmospheric Environment, 43, 6238-6253.

Baik, J. J and J. J. Kim, 2002: On the escape of pollutants from urban street canyons. Atmospheric Environment, 36, 527-536.

Baker, J., H. L. Walker, X. Cai, 2004: A study of the dispersion and transport of reactive pollutants in and above street canyons – a large eddy simulation. Atmospheric Environment, 38, 6883-6892.

Belcher, S.E., O. Coceal, E.V. Goulart, A.C. Rudd and A.G. Robins, 2015: Processes controlling atmospheric dispersion through city centres. Journal of Fluid Mechanics, 763, 51-81.
Benson, R.A. and D. S. McRae, 1991: A solution adaptive mesh algorithm for dynamic/static refinement of two and three dimensional grids: Proceedings of the 3rd International Conference on Numerical Grid Generation in Computational Field simulations, Barcelona, Spain, 1991.
Bentham, T., 2004: PhD thesis, Imperial College, London.
Bernal Castro, C.A. 2015: Dispersion of ait pollutants in central London. Master Thesis, School of Built Environment, London South Bank University, London, UK.
Boganegra, L. 2016: State of the art modelling of air flows and pollution around a building complex in central London, UK. Master Thesis, School of Built Environment, London South Bank University, UK.
Carpentieri, M and A.G. Robins, 2015: Influence of urban morphology on air flow over building arrays. Journal of Wind Engineering and Industrial Aerodynamics, 145, pp. 61-74.
Caton, F. and R. E. Britter and S. Dalziel, 2003: Dispersion mechanisms in a street canyon. Atmospheric Environment, 37: 693-702.
Coceal, O., A. Dobre, T. Thomas, and S. Belcher, 2007: Journal of Fluid Mech., 589:375–409.
Coirier, W., D. Fricker, M. Furmanczyk, and S. Kim, 2005: A computational fluid dynamics approach for urban area transport and dispersion modeling. Environmental Fluid Mechanics, 5:443-479.
Constantinescu, E., A. Sandu and G. Carmichael, 2008: Modelling atmospheric chemistry and transport with dynamic adaptive resolution. Comput Geosci, 12:133-151.
Cui, D.J., Mak, C.M., Kwok, K.C.S., and Ai, Z.T. 2016. CFD simulation of the effect of an upstream building on the inter-unit dispersion in a multi-story building in two wind directions. J. Wind. Eng. Ind. Aerodyn. 150, 31-41.
Di Sabatino, S., R.B. Buccolieri, B. Pulvirenti and R.E. Britter, 2008: Flow and pollutant dispersion in street canyons using FLUENT and ADMS-Urban. Environ Model Assess, 13:369-381.
Germano, M., U. Piomelli, P. Moin and W. H. Cabot, 1991: A dynamic subgrid-scale eddy viscosity model. Physics of Fluids A, 3, 1760.
Ghorai, S., A. Tomlin and M. Berzins, 2000: Resolution of pollutant concentrations in the boundary layer using a fully 3d adaptive gridding technique. Atmospheric Environment, 34:2851-2863.
Gorman, G., C. Pain, C. Oliveira, A. Umpleby, and A. Goddard, 2003: International Conference on Supercomputing in Nuclear Applications.
Gromke, C. and Blocken, B. 2015. Influence of avenue-trees on air quality at the urban neighbourhood scale: Part I: Quality assurance studies and turbulent Schmidt number analysis for RANS CFD simulations. Environmental Pollution, 196, 214-223.
Hong, B. and Lin, B. 2015. Numerical Studies of the outdoor wind environment and thermal comfort at pedestrian level in housing blocks with different building layout patterns and trees arrangement. Renewable Energy 73, 18-27.
Janhall, S. 2015. Review of urban vegetation and particle air pollution – deposition and dispersion. Atmospheric Environment, 105, 130 -137.
Jarrin, N., Benhamadouche, S., Laurence, D., and Prosser,R. 2006. A synthetic eddy-method for generating inflow conditions for large-eddy simulations," International Journal of Heat and Fluid Flow, vol. 27, pp. 585– 593, 2006.
Kastner-Klein, P., R. Berkowicz and R.E. Britter, 2004: The influence of street architecture on flow and dispersion in street canyons. Meteorol Atmos Phys, 87:121-131.
Kim, J.J. and J.J Baik, 2003: Effects of inflow turbulence intensity on how and pollutant dispersion in an urban street canyon. Journal of Wind Engineering and Industrial Aerodynamics, 91:309-329.
Kleissl, J., V. Kumar, C. Meneveau, M.B. Parlange, 2006: Numerical study of dynamic Smagorinsky models in large eddy simulation of the atmospheric boundary layer: validation in stable and unstable conditions. Water Resour Rese 42: W06D10.
Luo, K., Yu, H., Dai, Z., Fang, M and Fan, J. 2016. CFD simulations of flow and dust dispersion in a realistic urban area. Engineering Applications of Computational Fluid Mechanics 10:1, 229-243, DOI: 10.1080/19942060.2016.1150205.
Milliez, M. and B. Carissimo, 2007: Numerical simulations of pollutant dispersion in an idealized urban area for different meteorological conditions. Boundary Layer Meteorol. 122:321-342.
Pavageau, M. and M. Schatzmann, 1999: Wind tunnel measurements of concentration fluctuations in an urban street canyon. Atmospheric Environment, 33:3961-3971.
Pain, C., A. Umpleby, C. de Oliveira and A. Goddard, 2001: Computer Methods in Applied Mechanics and Engineering, 190:3771–96.
Pavlidis (2010) Ph.D. Thesis, Imperial College London.
Piomelli (1999): Large Eddy Simulations: Achievements and challenges. Prof. Aerospace Sci, 35(4), 335-362.
Porte-Agel, F. 2004: A scale-dependent dynamic model for scalar transport in large-eddy simulations of the atmospheric boundary layer. Boundary-Layer Meteorol 112: 81-105.

Pope, S. 2000: Turbulent flows. Cambridge University Press.

Robins (2013). Personal Communication.

Solazzo, E. and R. Britter, 2007: Transfer processes in a simulated urban street canyon. Boundary-Layer Meteorol, 124:43-60.

Srivastava, R., D. McRae, and M. Odman, 2001a: Simulation of a reacting pollutant puff using an adaptive grid algorithm. Journal of Geophysical Research, 106:24245-24257.

Srivastava, R., D. McRae, and M. Odman, 2001b: Simulation of dispersion of a power plant plume using an adaptive grid algorithm. Atmospheric Environment, 35:4801-4818.

Tong, Z., Chen, Y., Malkawi, A., Adamkiewicz, G. and Spengler, J.D. 2016. Quantifying the impact of traffic-related air pollution on the indoor air quality of a naturally ventilated building. Environment International 89-90, 138-146.

Walton A., and A.Y.S. Cheng, 2002: Large Eddy simulation of pollution dispersion in an urban street canyon: Part II: idealised canyon simulation.

Wissink, A., K. Chand, B. Kosovic, S. Chan, M. Berger and F.K. Chow, 2005: Adaptive Urban Dispersion Integrated Model. 86th American Meteorological Society Annual Meeting, Atlanta, GA, USA. UCRL-PROC-216813.

Zhang, N., DU, Y., Miao, S. 2016. A microscale model for air pollution dispersion simulation in urban areas: presentation of the model and performance over a single building. Advanced in Atmospheric Sciences, 33, 184-192.

Zhou, Y. and S. Hanna, 2007: Along-wind dispersion of puffs released in a built-up urban area. Boundary-Layer Meteorol, 125:469-486.

APPENDIX A: The Large Eddy Simulation method with an anisotropic eddy viscosity model.

The three-dimensional filtered Navier Stokes equations for mass continuity and momentum, as follows:

(Eq. 1) Mass Continuity $$\frac{\partial \tilde{u}_i}{\partial x_i} = 0$$

(Eq. 2) Momentum $$\frac{\partial \tilde{u}_i}{\partial t} + \tilde{u}_j \frac{\partial \tilde{u}_i}{\partial x_j} = -\frac{1}{\rho}\frac{\partial \tilde{P}}{\partial x_i} + \frac{\partial}{\partial x_j}\left[\upsilon\left(\frac{\partial \tilde{u}_i}{\partial x_j} + \frac{\partial \tilde{u}_j}{\partial x_i}\right) + \tau_{ij}\right]$$

where $\tilde{u}_i$ is the resolved velocity field, $\tilde{P}_i$ is the resolved fluid pressure field, ρ is the fluid density (incompressible fluid), υ is the kinematic viscosity of the fluid (air in our case) and τ_{ij} is the sub-grid scale tensor.

The key and novel component in the implementation of the standard LES equations within FLUIDITY is the anisotropic eddy viscosity tensor, $\nu_{t(ij)} = (C_s \Delta)^2 \tilde{S}_{ij}$ linked to the adaptive mesh, where C_s is the Smagorisnki constant (C_s is set at the constant value of 0.11 within the models); Δ is the filter length – dependent on the local element size as shown further below; and $\tilde{S}_{ij}$ is the local strain rate component, determined through the expression:

(Eq. 3) Local strain rate component $\tilde{S}_{ij}$

$$\tilde{S}_{ij} = \left(\frac{\partial \tilde{u}_i}{\partial x_j} + \frac{\partial \tilde{u}_j}{\partial x_i}\right)$$

One of the novelties of the implemented LES code lies in the fact that local filter length Δ depends on the local element size (h_ζ, h_η, h_ξ) according to the relationship $\Delta = 2 \times (h_\zeta, h_\eta, h_\xi)$ (in the local element co-ordinate system). Rotational transformations V^T and V are used to transform from the local co-ordinate system to the global one, leading to the inverse of a mesh-adaptivity metric M given by:

(Eq. 4) $$M^{-1} = V^T \begin{bmatrix} h_\zeta^2 & 0 & 0 \\ 0 & h_\eta^2 & 0 \\ 0 & 0 & h_\xi^2 \end{bmatrix} V$$

Thus, the anisotropic eddy viscosity tensor is determined through the expression:

(Eq. 5) $$\nu_t = C_s^2 |\tilde{S}| V^T \begin{bmatrix} \Delta_\zeta^2 & 0 & 0 \\ 0 & \Delta_\eta^2 & 0 \\ 0 & 0 & \Delta_\xi^2 \end{bmatrix} V = 4C_s^2 |\tilde{S}| \underbrace{V^T \begin{bmatrix} h_\zeta^2 & 0 & 0 \\ 0 & h_\eta^2 & 0 \\ 0 & 0 & h_\xi^2 \end{bmatrix} V}_{M^{-1}}$$

Whilst the spatial gradients of the stress tensor components are determined through the expression:

$$\frac{\partial \tau_{ij}}{\partial x_{ij}} = \frac{\partial}{\partial x_{ij}}\left[\nu_{jk}\frac{\partial u_j}{\partial x_k}\right]$$

(Eq. 6)

ADDITIONA FIGURES

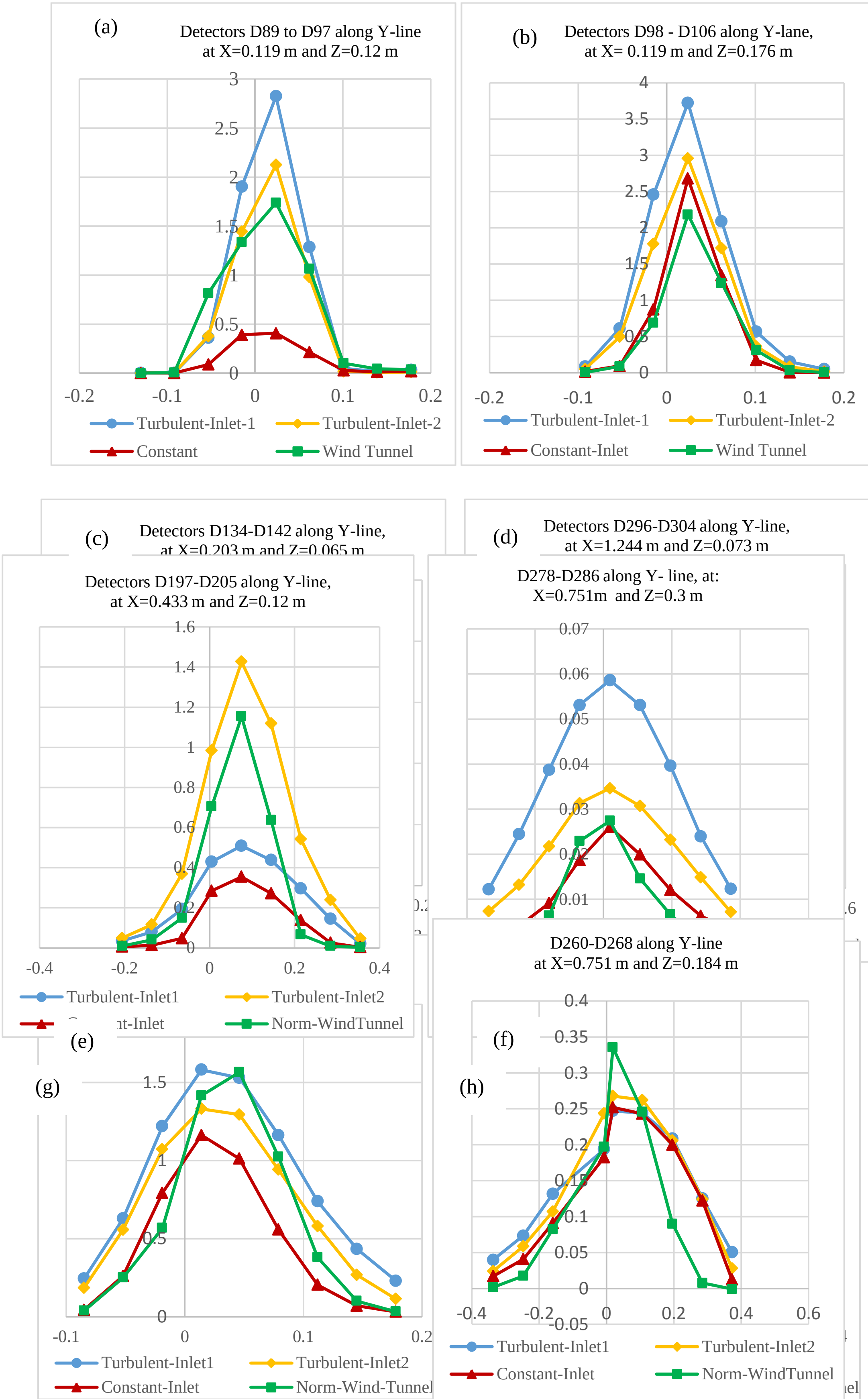

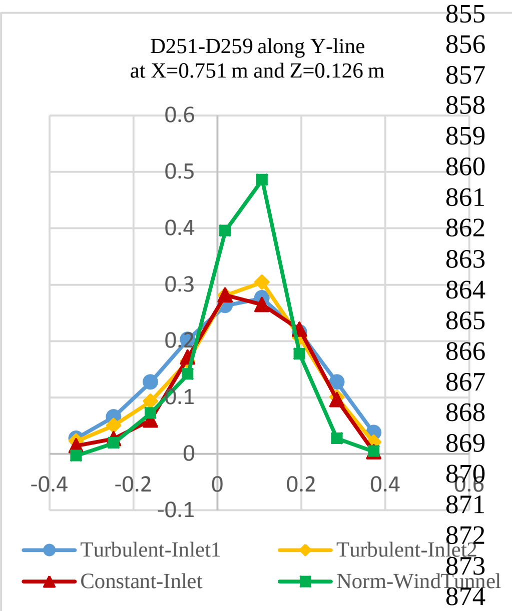

Fig. 4 Ten plots (a) to (j) showing the comparison of *normalised mean concentrations* between wind tunnel data and FLUIDITY simulations for a number of detectors along different Y-lines. (location of detectors is indicated in each plot).

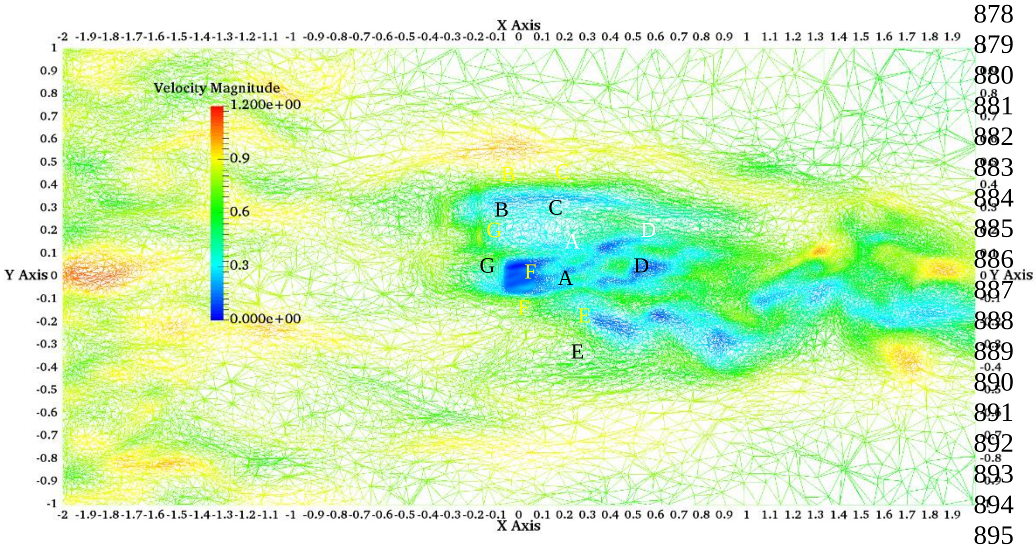

(a) Case1 at height Z=0.1508

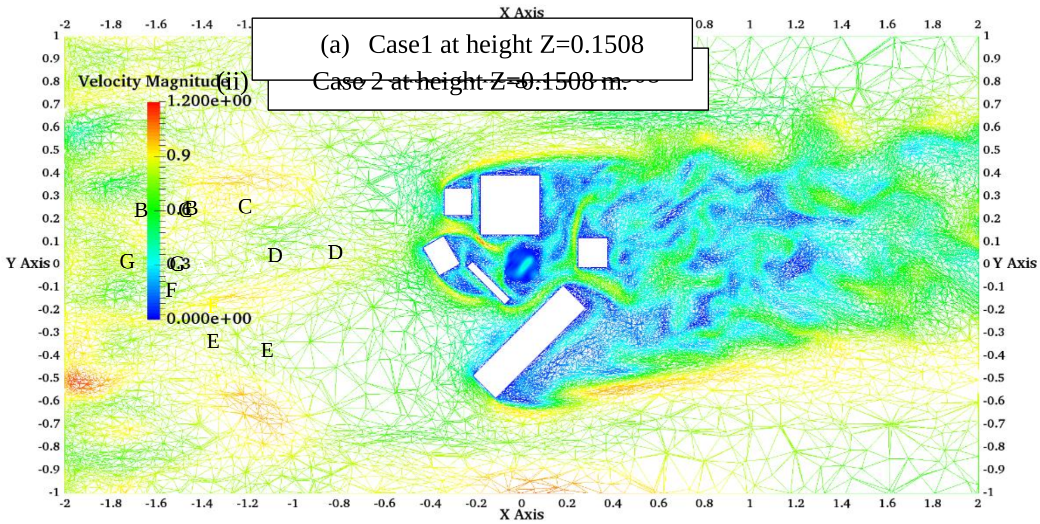

(ii) Case 2 at height Z=0.1508 m.

(c) Case1 at height Z=0.1508 m.

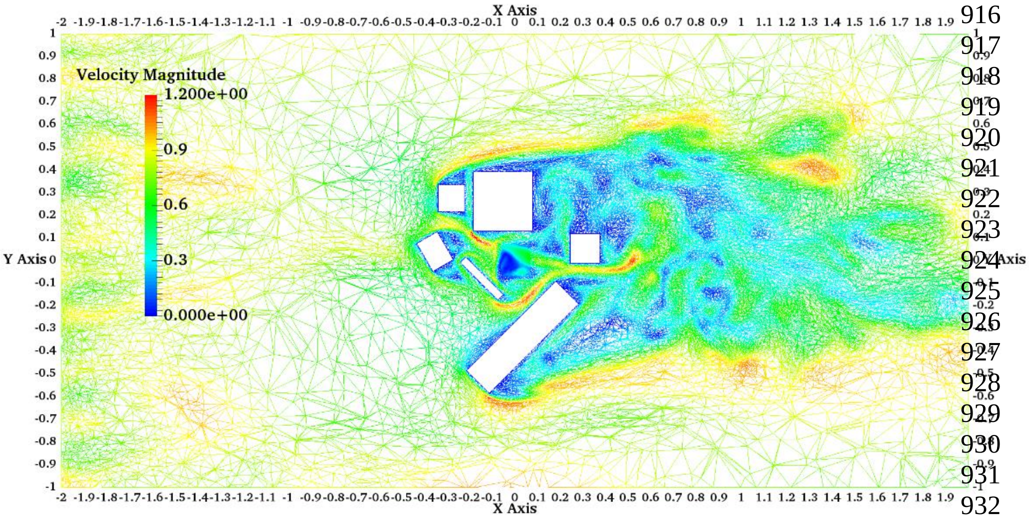

Fig. 5a Horizontal plane (X-Y) view at Z=0.1508 m of the Turbulent Velocity fields in wireframe presentation for the three cases: (i) Case 1; (ii) Case 2; (iii) Case 3.

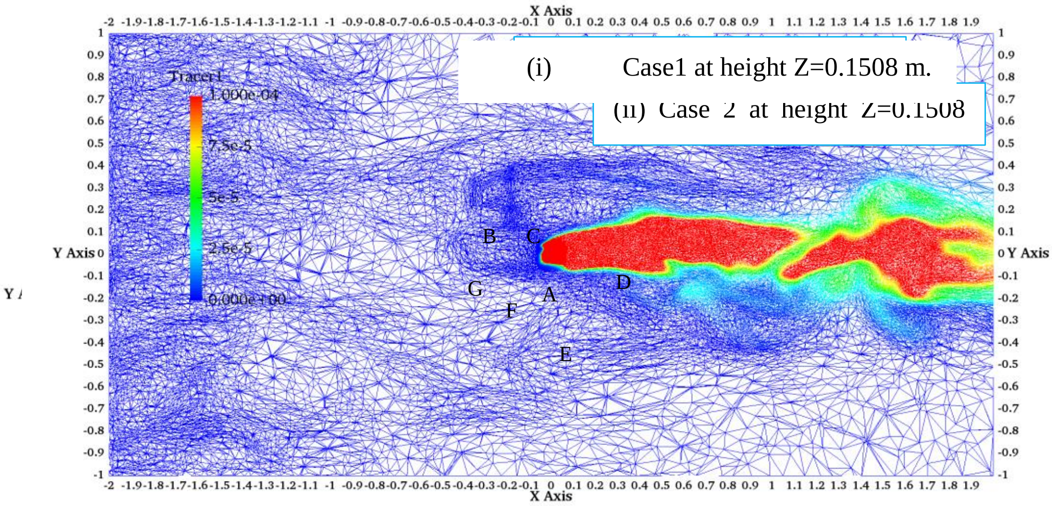

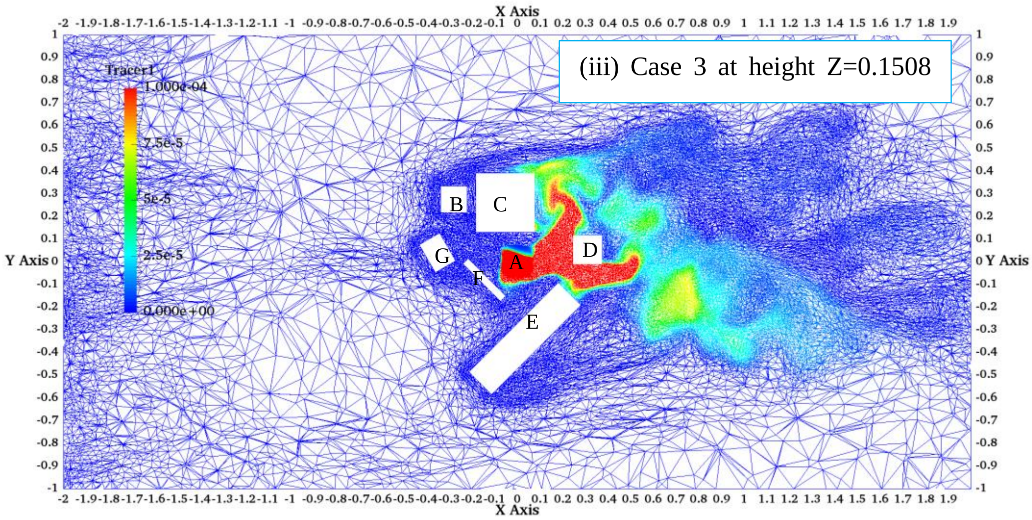

Fig. 5b Horizontal plane (X-Y) view at Z=0.1508 m of Tracer dispersion with the Adaptive meshes for the three cases:(i) Case 1; (ii) Case 2; (iii) Case 3. No of elements ~ 1000000. The effect of the taller buildings is clearly seen.

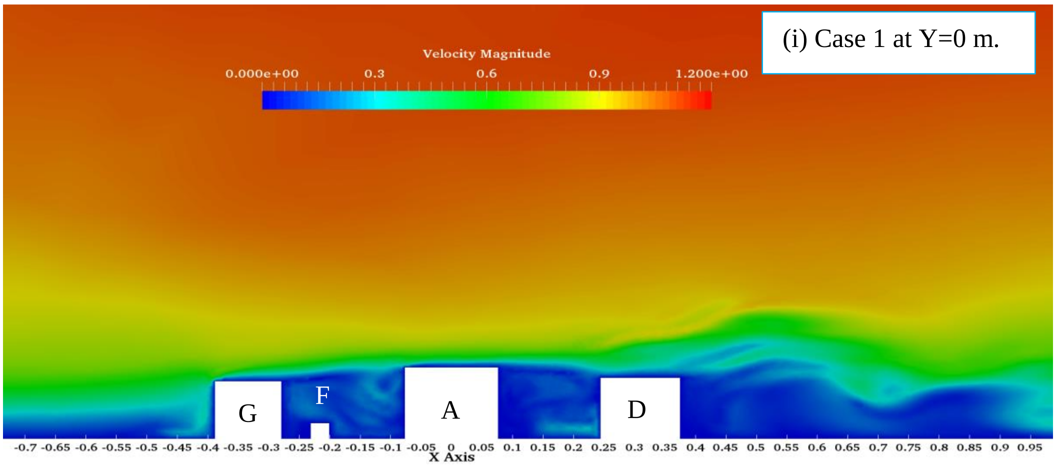

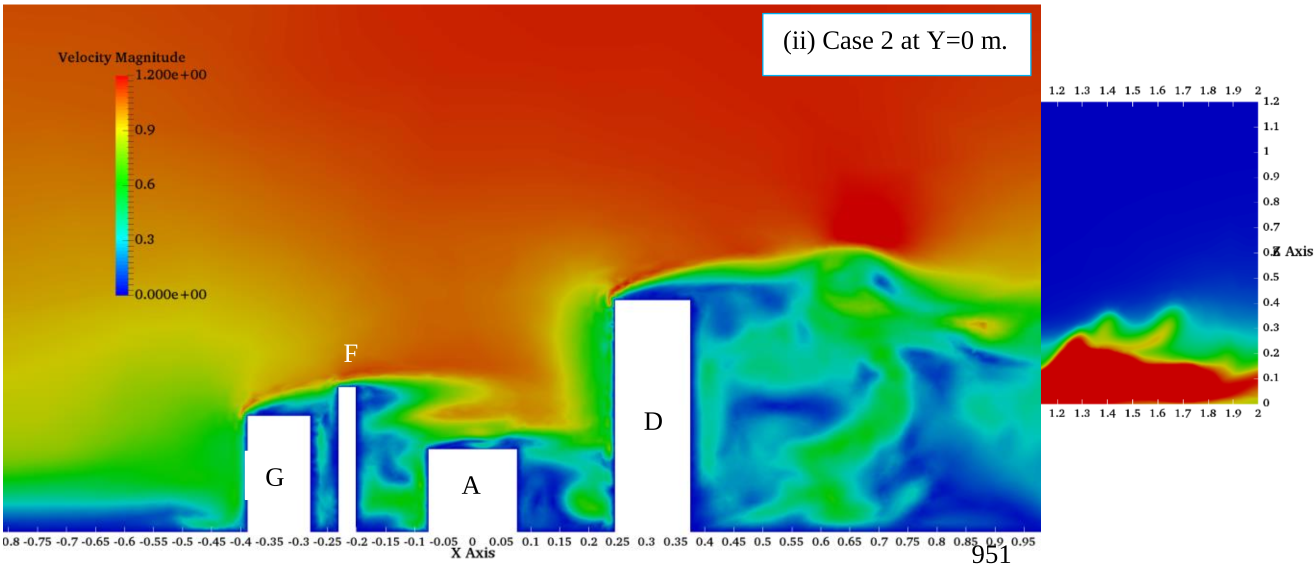

Fig. 6a Vertical plane (X-Z) view through the centre of the domain (Y=0.0 m), showing the interesting

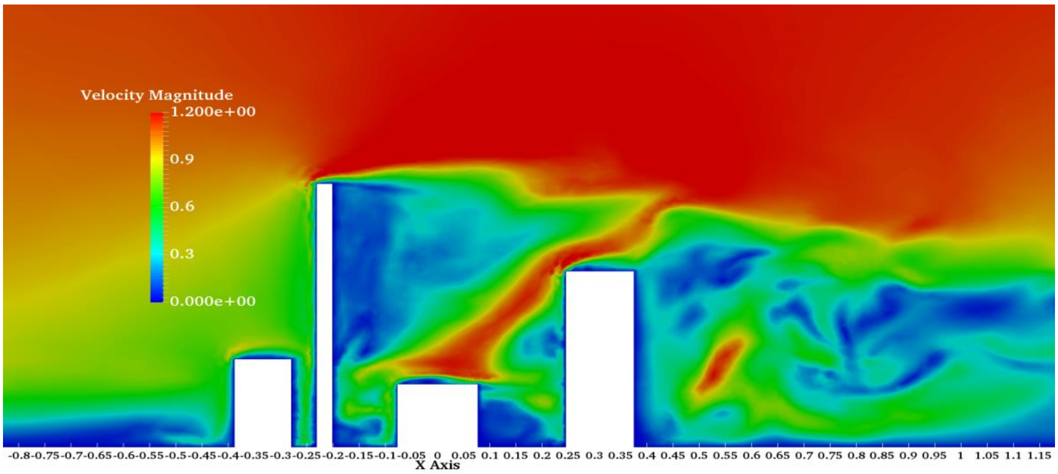

Variations of the **Velocity fields** for the three cases: (i) Case 1; (ii) Case 2; (iii) Case 3.

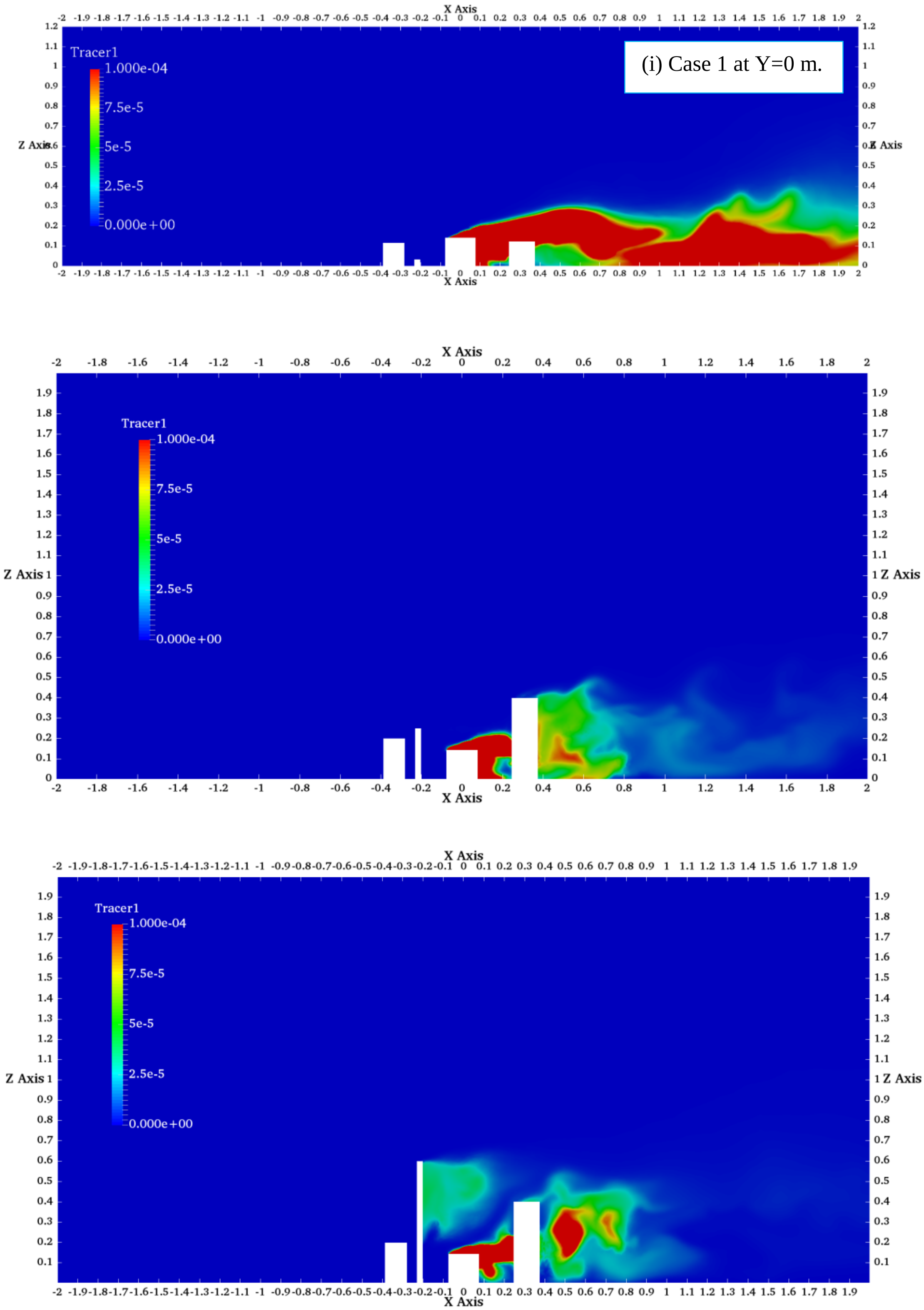

Fig. 6b Vertical plane (X-Z) view through the centre of the domain (Y=0), showing the interesting Variations of the **Tracer Dispersion** for the three cases: (i) Case 1; (ii) Case 2; (iii) Case 3. The effect of the height of the height of the buildings is clearly seen.

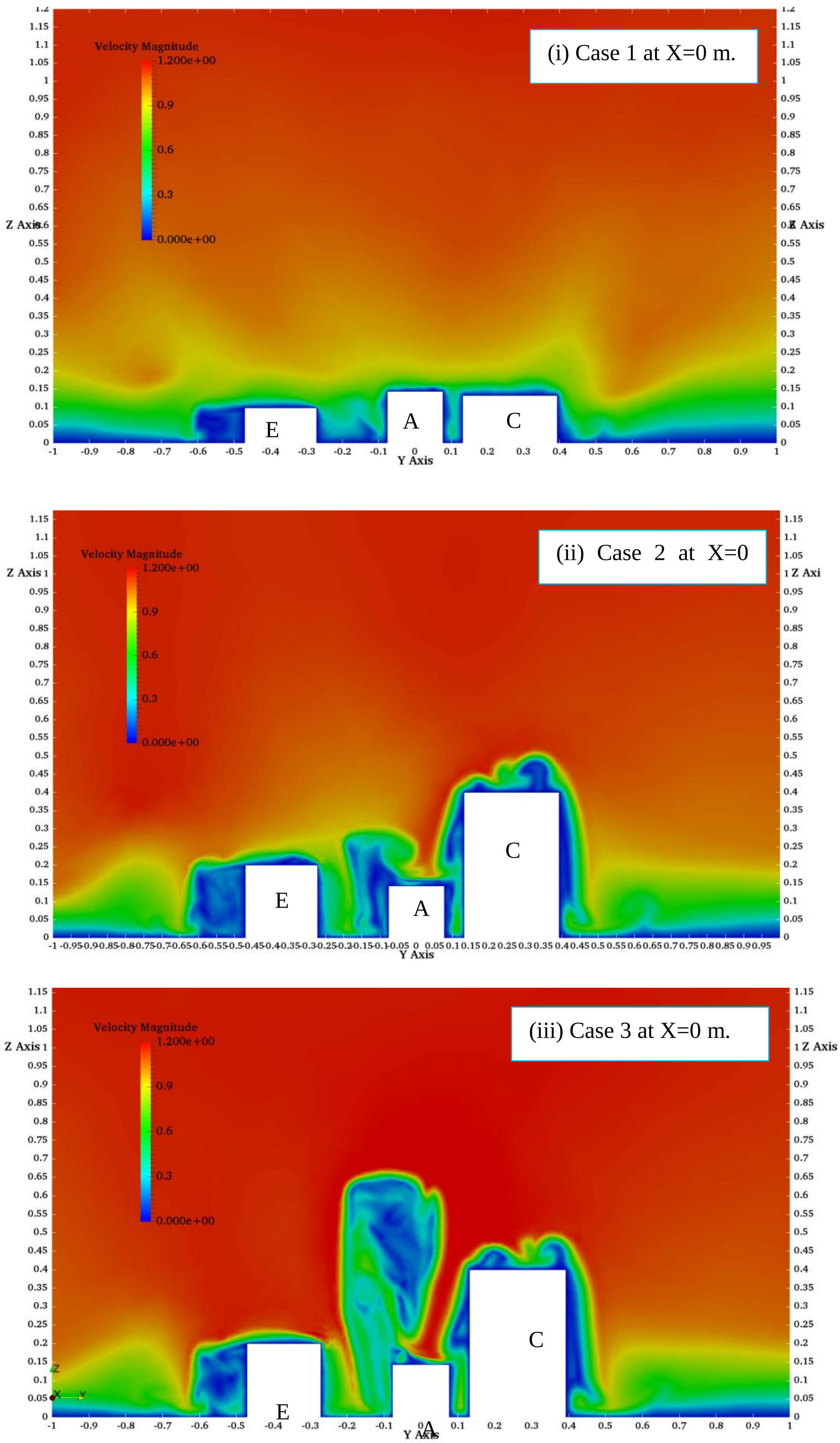

Fig. 7a Vertical plane (Y-Z) view through the centre of the domain (X=0), showing **the Velocity Variations** for the three cases: (i) Case 1; (ii) Case 2; (iii) Case 3.
The effect of the height of the height of the buildings is clearly seen

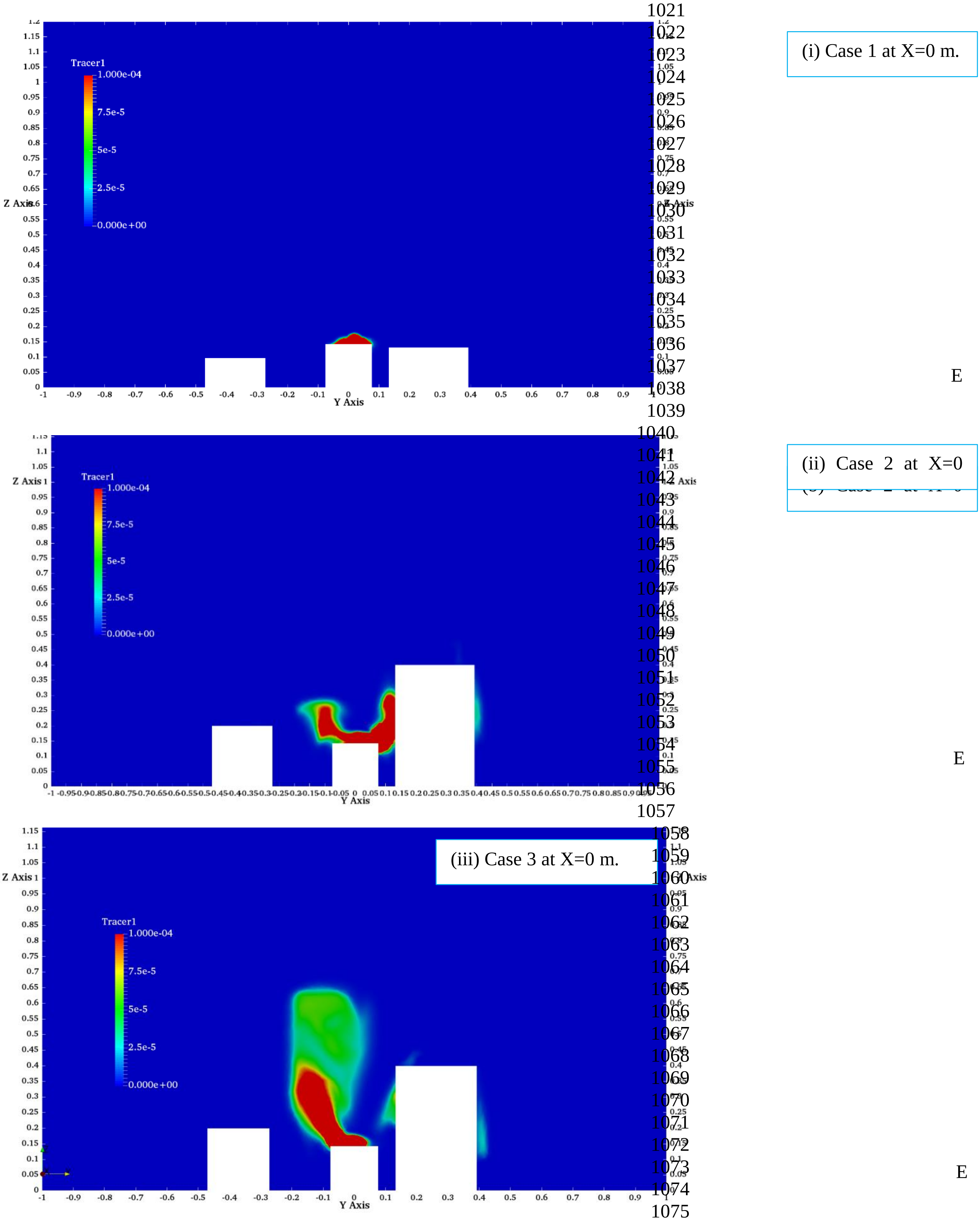

Fig. 7b Vertical plane (Y-Z) view through the centre of the domain (X=0.0m), showing the interesting Variations of the **Tracer Dispersion** for the three cases: (i) Case 1; (ii) Case 2; (iii) Case 3. The effect of the height of the height of the buildings is clearly seen

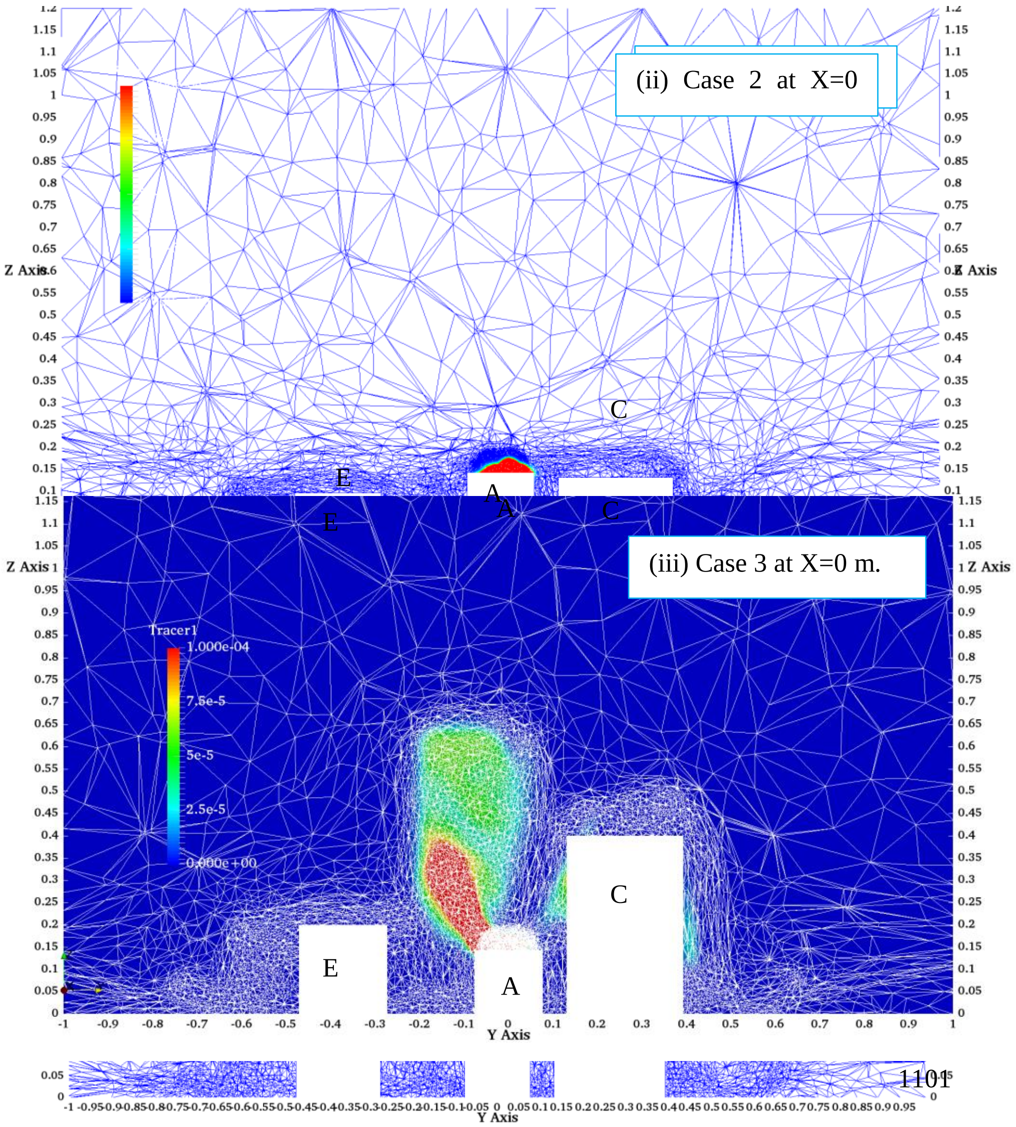

Fig. 7c

Vertical plane (Y-Z) view through the centre of the domain (X=0.0m) of the **Tracer Dispersion with the Adaptive meshes** for the three cases: (i) Case 1; (ii) Case 2; (iii) Case 3.
The effect of the height of the height of the buildings is clearly seen.

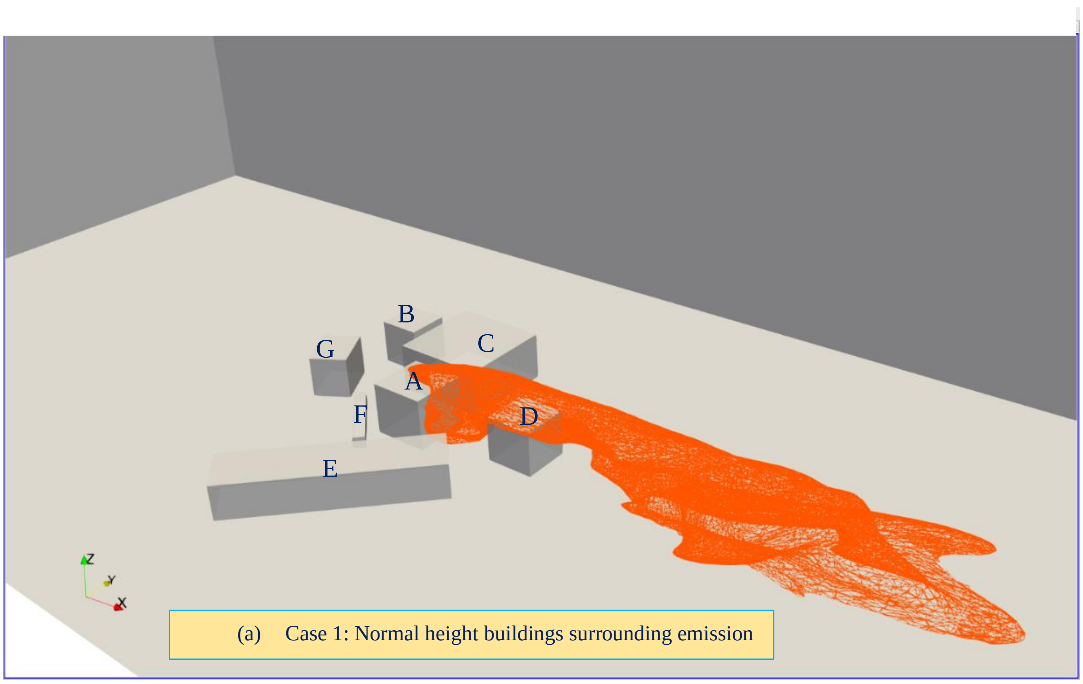

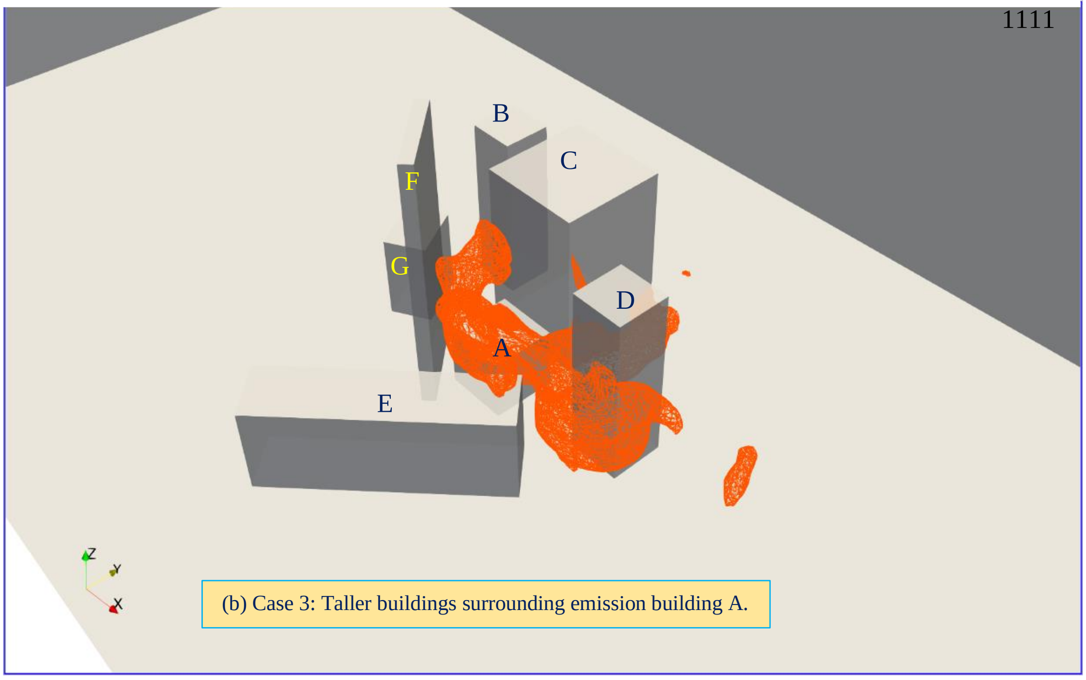

(b) Case 3: Taller buildings surrounding emission building A.

Fig. 8 Concentration Iso-surfaces for Cases 1 and Case 3, showing how the presence of tall buildings affects pollution dispersion within a local neighbourhood. The effect of the taller buildings is clearly captured in the simulations – with the concentration field remaining close to the building area in Case 3, as opposed to dispersing away as in scenario Case 1. *Concentration Isosurface = 0.0001*.

TABLES

Building Identification	**Building Height (m)** Wind tunnel Case 1	**Building Height (m)** Case 2	**Building Height (m)** Case 3
A (Garden building)	**0.1428**	**0.1428**	**0.1428**
B (Park building)	0.1238	0.4	0.4
C (Exhibition building)	0.1315	0.4	0.4
D (High street building)	0.1228	0.4	0.4
E (Melbury building)	0.0971	0.2	0.2
F (Garage building)	0.0315	0.2	0.2
G (Park close building)	0.1152	0.25	0.6

Table 1. Dimensions of building heights for different simulation scenarios.

Detector No	**% Error**	**Detector No**	**% Error**
90	12	155	3
91	10	156	19
92	24	281	27
93	7	282	5

94	14	283	22
101	8	284	30
102	18	540	37
103	21	543	16
104	7	545	3
153	5	546	24
154	22	548	1

Table 2. Percentage errors of mean concentrations for several detectors.